Available online at www.sciencedirect.com
ScienceDirect
Journal of Sound and Vibration 322 (2009) 901–925
JOURNAL OF SOUND AND VIBRATION
www.elsevier.com/locate/jsvi

Damping and induced damping of a lightweight sandwich panel with simple and complex attachments

S.C. Conlon*, S.A. Hambric

Applied Research Laboratory, The Pennsylvania State University, PO Box 30, State College, PA 16804-0030, USA

Received 4 January 2008; received in revised form 24 November 2008; accepted 2 December 2008
Handling Editor: C.L. Morfey
Available online 20 January 2009

Abstract

Accurately estimating a structure's broadband response is highly dependent on a proper characterization of the system's internal damping as well as induced (or effective) damping when coupled systems are considered. In many aerospace and related applications a primary or master structure is loaded with equipment or substructures. The effects of these attachments on the master structure are often poorly understood and frequently overlooked, but in many cases can dominate the master structure's response. In this work various measures of damping of a lightweight aerospace panel (aluminum sandwich honeycomb core panel) with simple (lumped mass) and complex (electronic equipment) attachments are investigated using experimental techniques and simple statistical energy analysis models. The panel's various measures of damping in steady-state conditions are defined and explored. The panels with simple and complex attachments are experimentally evaluated using power injection methods. The results show that at different frequencies the simple panel's response is controlled by internal and then acoustic radiation damping. The complex attachment's induced damping effects, however, can far exceed both the structure internal and acoustic radiation components. A range of complex attachment configurations are evaluated and general design assessment procedures developed for use by designers. Future work is planned to explore the systems transient response and derived parameters, as well as investigate the effects when the attachment mass varies over a greater range of values, a realistic condition applicable to many aerospace systems.

1. Introduction

Many acoustics and vibration problems of practical interest deal with systems and the interactions of several or many such systems, that are not amenable to closed form analytical models or solutions from classical mechanics. Examples are numerous in the aerospace, marine and automotive as well as other transportation industries. Quite often these systems deal with combinations of well-defined master structures coupled to many complex attachments or substructures with the combined structural systems interacting with a surrounding acoustic medium.

*Corresponding author.
E-mail address: scc135@only.arl.psu.edu (S.C. Conlon).

0022-460X/$ - see front matter © 2008 Elsevier Ltd. All rights reserved.
doi:10.1016/j.jsv.2008.12.006

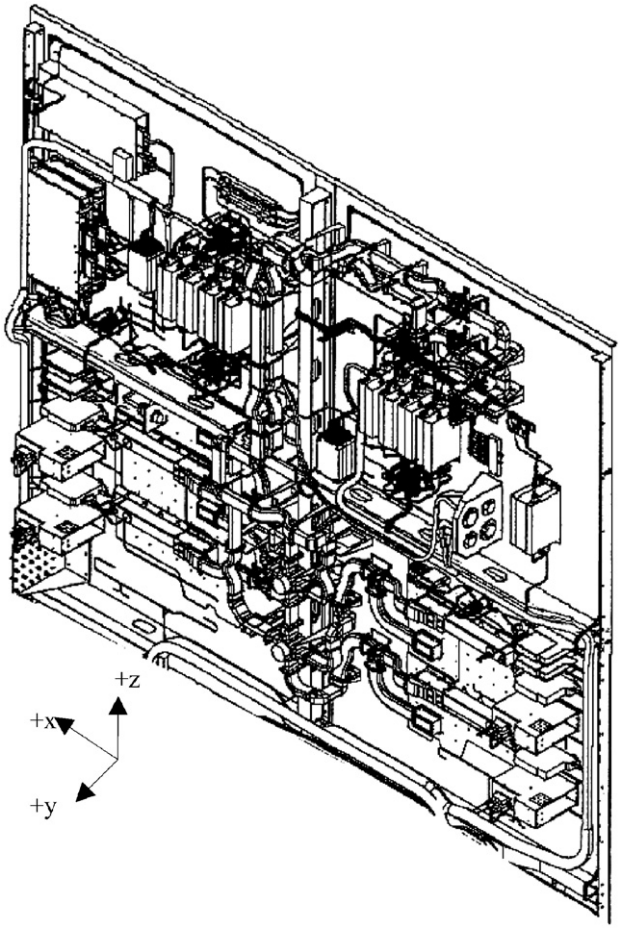

Fig. 1. Satellite equipment panel. Underlying sandwich honeycomb core panel with attached complex electronics.

A specific example of such a system is a communications satellite equipment panel [1] such as shown in Fig. 1. The basic underlying structures of these equipment panels are very lightweight, typically consisting of a sandwich honeycomb core construction. The panels have added stiffeners and other reinforcements along with the (structurally) complex electronics that are mounted to them. It is not uncommon for the total mass of the loaded panel to be up to 10 times (or more) that of the basic sandwich panel.

When these equipment panels are subjected to intense acoustic loading, as they are during qualification testing and launch, they can respond at vibration levels that can damage the high-value equipment causing loss of electrical functionality. The equipment attached to these panels can have significant effects on the structural acoustic coupling as well as on the effective modal vibration and damping characteristics of the underlying structural system. The effects of the complex equipment on the response of the panel master structure are shown in the example of Fig. 2, where vibration responses at 2000 Hz of the equipment loaded panel from Fig. 1 are approximately 24 dB below that of the same panel with non-resonant "lumped mass" attachments.

There is little data available in terms of published damping measurements for satellite or spacecraft structures that would quantify the effects shown in Fig. 2. Most of what has been published pertains to low frequencies and focuses on low-order modal responses typically below 100 Hz (and sometimes much lower). The European Space Agency's Structural Acoustics Design Manual [2] suggests that the equipment increases the underlying panel damping by 20–25% but also indicates "little practical information is available, except that adding equipment items will tend to increase the damping of the platform panel" and "damping values in built-up conditions are poorly known and under investigation".

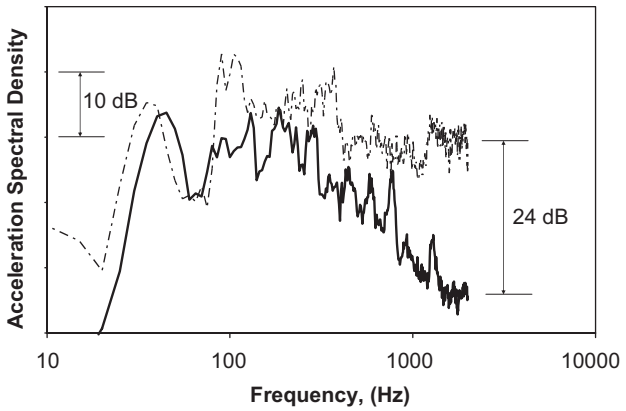

Fig. 2. Panel with complex attachments vs. panel with simple attachments in situ vibration responses (—·— panel response with lumped masses 17.2 g-rms overall, — panel response with electronic equipment attachments 5.8 g-rms overall). The vibration absorption effects of the complex attachments are significant at the higher frequencies.

The effective or induced frequency-dependent damping caused by complicated substructures attached to a master structure, was an important concept investigated in detail by Soize [3] and many others in subsequent years [4–7]. These early publications, which termed the complex attachments "fuzzy" structures, reintroduced the important, often elusive and well debated concept of effective or induced damping as was described earlier by Maidanik [8,9], Brooks and Maidanik [10], Bies and Hamid [11], Sun and Richards [12] and Sun et al. [13].

In fuzzy structures analysis, as presented by Soize [3], the system is divided into the master structure, which is the portion of the structure that is known and amenable to deterministic modeling such as finite element modeling and the fuzzy substructure, which consists of one or several resonant lightly damped substructures with high modal density coupled or connected to the master structure. The fuzzy substructures are too complicated or not well enough understood to model using traditional techniques. For these substructures Soize used a stochastic model defining a fuzzy substructure by three parameters, which are the participating mass coefficient, the internal damping rate and the modal density. The probability distribution of the eigenfrequencies of such a fuzzy substructure is constructed using the modal density and yields a non-uniform distribution. In addition, since the three parameters are uncertain, these parameters are modeled by random variables whose probability distributions are constructed using information theory yielding uniform distributions. This technique adds the attachment effects as boundary impedances thus not increasing the master structure model degrees of freedom (dof).

Alternatively, other investigators replaced the attachment stochastic model with a Monte Carlo solution using a distribution of sets of deterministic attached substructure properties (typically lightly damped simple oscillators). The work by Pierce et al. [4] (PSR method) dealt with the specific case of a baffled rectangular plate with an attached system of spring mass oscillators (fluid is on the side of the plate opposite the oscillators.) The PSR method introduces a fuzzy mass–frequency distribution which is the product of the participating mass coefficient with the modal density of the Soize fuzzy structure theory and is assumed to follow a Rayleigh distribution. The key result of Pierce et al.'s work is that, for small values of attachment damping, the added apparent damping to the master structure (plate) is relatively independent of the attachment internal damping and dependent on the critical mass–frequency distribution parameter.

Strasberg and Feit [5] started with a much simpler deterministic model where the master structure was a large rigid mass and the attached substructures were a number of sprung small masses. They showed that the induced damping (in the limit of small attachment damping) to the large mass was predominantly dependent on the total effective attached mass resonating in the band centered at the frequency of (the master structure) vibration, with this limit dependent on maintaining a condition of attachment modal overlap. Strasberg and Feit then addressed a continuous system and showed a similar result as the PSR method in that the induced damping is shown to depend on the rate of change of incremental mass to incremental (antiresonance) frequency of the attached substructure. Conceptually these results make sense in that the dominant effective damping mechanism to the master structure is the transfer of kinetic energy to the attached oscillators and thus

the attachment resonance distribution in a given band is the dominant parameter which in turn is a function of the oscillator mass, as opposed to internal damping, provided that sufficient modal overlap is maintained.

More recently Maidanik and Dickey [14,15], Maidanik and Becker [16–18] and Maidanik [19] have investigated the damping and input power effects of coupled systems. Akay and Xu [20] and Koc et al. [21] have examined the effects from the perspective of optimal sets of energy sinks consisting of optimized frequency distributions of attached oscillators. Although these methods have generated continued interest in what are effectively vibration absorbers they still retain a major issue with their practical implementation in that there is no way to generally characterize the boundary input impedance of many realistic complex substructures of interest.

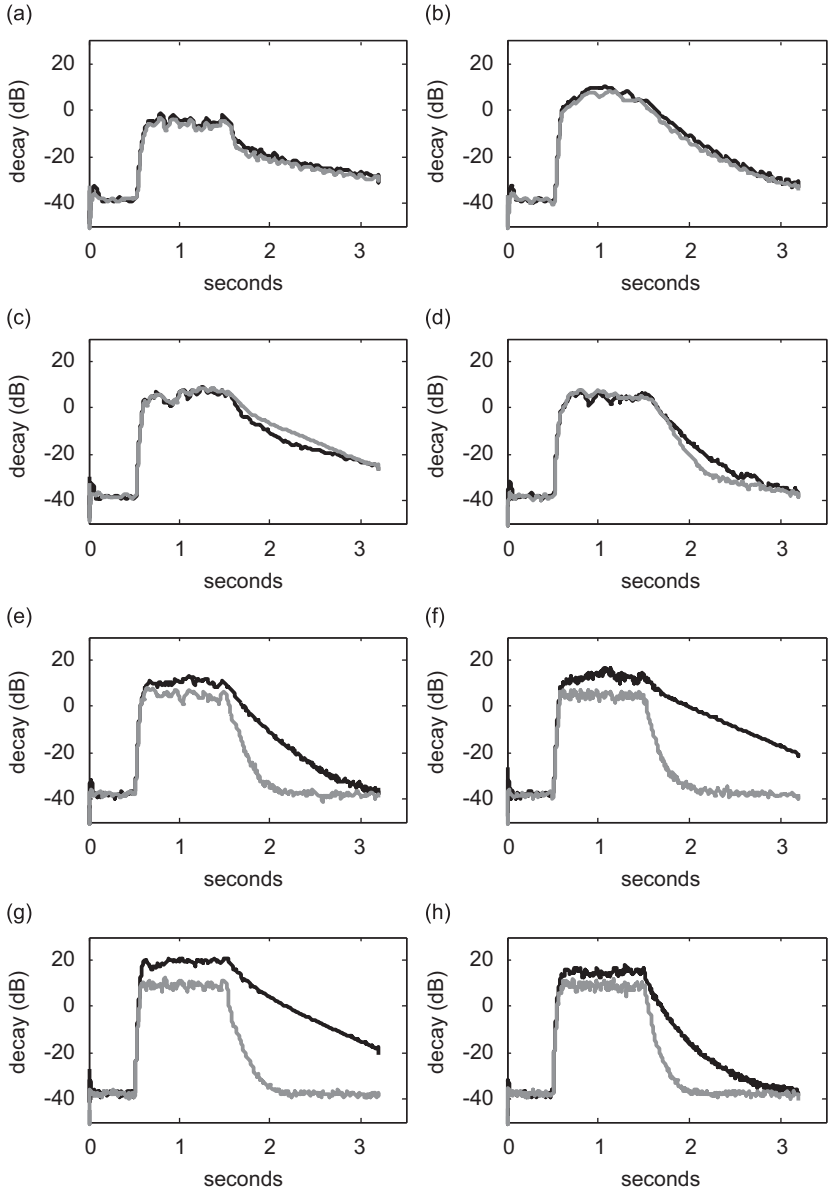

Fig. 3. Panel with complex attachments and panel with simple attachments vibration decay envelopes, 50–250 Hz one-third octave bands: (a) 50 Hz, (b) 63 Hz, (c) 80 Hz, (d) 100 Hz, (e) 125 Hz, (f) 160 Hz, (g) 200 Hz and (h) 250 Hz (—— panel with complex attachments {electronic equipment}, —— panel with simple attachments {lumped masses}). The vibration absorption effects of the resonant complex attachments are the dominant panel loss mechanism from 125 to 315 Hz.

One of the most significant differences between the cited fuzzy structures works and this investigation is that typically the fuzzy structures investigations were limited to considering attached substructures typically of only 10% of the master structure mass (and on occasion perhaps as high as 20–40%) whereas in this investigation the attachment mass configurations are approximately equal to, as well as several factors times, that of the underlying panel structure mass. Note that from a practical design point of view these attachment to panel structure mass ratios would not be considered high, noting that for many equipment panel designs the complex attachment mass can easily be 10–20 times the underlying structure mass, but is of particular concern to designers due to the high amplitude responses experienced in use of this class of loaded panels. This raises

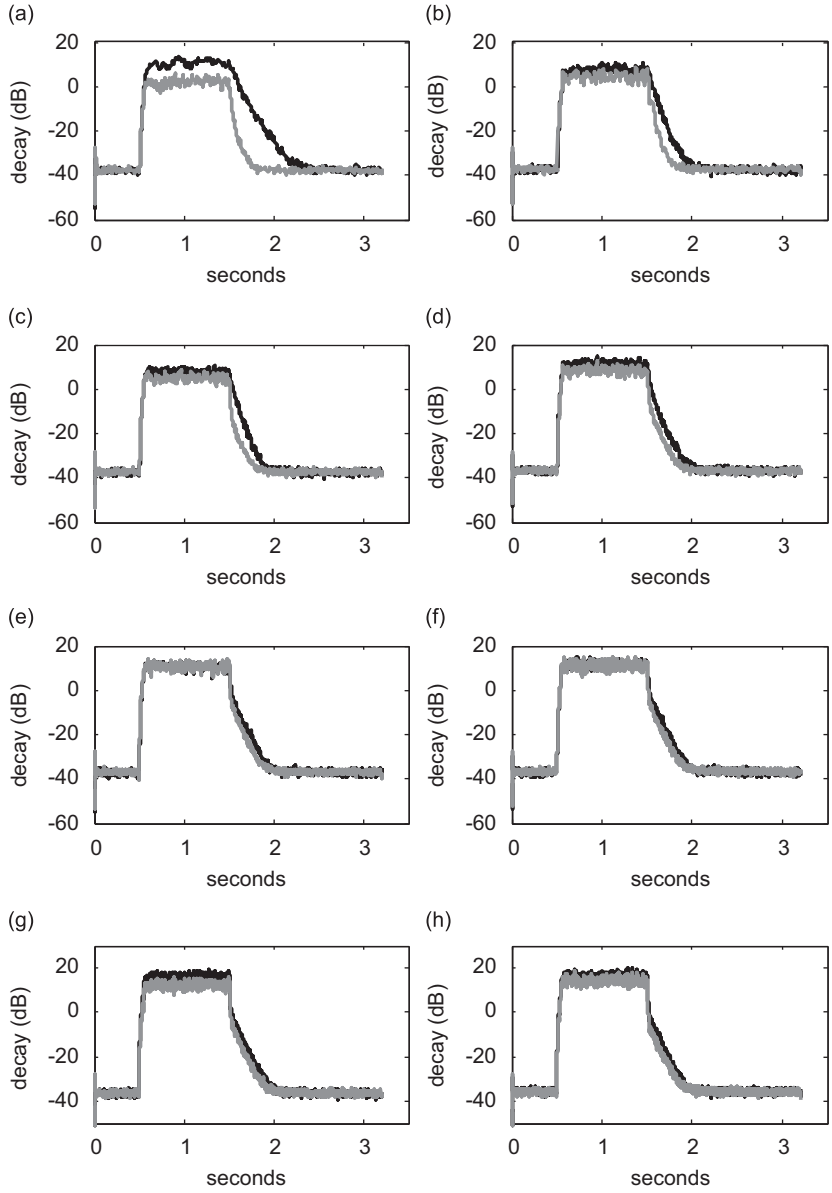

Fig. 4. Panel with complex attachments and panel with simple attachments vibration decay envelopes, 315–1600 Hz one-third octave bands: (a) 315 Hz, (b) 400 Hz, (c) 500 Hz, (d) 630 Hz, (e) 800 Hz, (f) 1000 Hz, (g) 1250 Hz and (h) 1600 Hz (—— panel with complex attachments {electronic equipment}, ▬▬ panel with simple attachments {lumped masses}). The vibration absorption effects of the resonant complex attachments are the dominant panel loss mechanism from 125 to 315 Hz. Above approximately 400 Hz the panel acoustic radiation losses are the dominant panel damping mechanism.

the question of whether the (maximum attachment mass) configurations investigated here even fit the previous concepts of a master structure with attached fuzzy substructures. One might speculate that with the fuzzy substructure mass being equal to or much greater than the master structure mass, that the reactive induced effects could significantly alter the underlying master structure characteristics, in addition to the already anticipated induced resistive effects that will be investigated here.

Figs. 3 and 4 compare two sets of panel free vibration decay measurements made on the panels, with simple and complex attachments, used in this investigation (the attachment total mass is approximately equal to the underlying panel structure mass.). The rates of decay or slopes of these curves are indicative of the panel system induced or effective damping (the panel coupled to the attachments as well as to the surrounding acoustic volume.) The curves show similar decay rates at the low frequencies. As the frequency increases, the response of the panel with complex attachments (electronic equipment) starts to decay more rapidly than that with the simple attachments (lumped mass) up to about 200 Hz where the resonant attachments have the maximum effect. Unlike the frequency domain curves shown in Fig. 2, which showed a continuing divergence between the responses of the panel with different attachments, Figs. 3 and 4 show the response of the panels converging above 200 Hz. This occurs because the frequency domain data comes from panels, with substantially more attached mass per area, where the induced damping of the panel with complex attachments is dominated by the attachments over all the high frequencies. However, the decay data differs in that it comes from panels with much lower attached mass per area, investigated in this work, where the (resonant) complex attachment induced damping is significant at 200 Hz but is overcome by the panel acoustic radiation damping at the higher frequencies (thus the decay curves converge). Note the panel (no attachments) critical frequency is approximately 560 Hz.

As illustrated in the presented examples, the complex attachments can have significant effects on the master structure's vibration response. In addition, the roles of the vibration control mechanisms can be further complicated by the system interaction with the acoustic medium in terms of radiation damping contributions to the overall effective damping. This investigation strives to examine and increase the understanding of the effects of simple and complex attachments and the roles of the significant damping mechanisms, on a class of panel structures through power injection experimentation and critical parameter derivations using simple statistical vibroacoustic models. The specific goals of this work focus on (1) establishing a model framework for assessing critical system vibroacoustic parameters, (2) the experimental procedures for assessing the parameters of interest and (3) assessing initial quantitative results for the critical parameters, as well as their interpretations and their implications of interest to designers. This work will provide the foundation for future investigations encompassing a wider range of hardware configurations of interest to designers.

2. Hardware and model definition

In this section the design details of the hardware used in the investigation are presented. In addition, the modeling approach and assumptions are defined which are used to develop the critical vibroacoustic parameter estimates of interest from the raw measurements.

2.1. Hardware description

The types of stiff lightweight aerospace structures investigated have relatively low critical frequencies due to their light weight and high cross-sectional radius of gyration, indicative of strong acoustic coupling, as well as complex attached (resonant) equipment, which also can have significant effects on the underlying structure in the form of induced damping and mass loading. It is how the underlying structure interacts with the surrounding acoustic field and the complex attachments that is of utmost interest in this investigation. This being the case, not only are the structure details of full scale but the attachments are as well. The electronic equipment are representative of the shapes, sizes and weights used in the satellite community (with associated internal circuit boards and piece part complexity) and are not amenable to deterministic broad frequency band modeling.

The approach taken in this work is to start with a simple baseline panel structure, measure its critical parameters and then add the complex attachments (electronic equipment). Also, simple attachments (lumped

masses) are attached to the panel to differentiate mass and damping effects of the complex attachments. This allows one to characterize the transition the parameters make as the structure transitions from an ideal uniform structure to a loaded structure with simple and also with complex, internals. It is the mid-frequency transition character and breadth that is of particular interest. The effects of the complex attachments are compared and contrasted to those of the simple attachments, emphasizing the effects between resonant and non-resonant (complex and simple) attachments.

The sandwich panel has 0.305 mm thick (0.012 in) aluminum facesheets and honeycomb core with a total panel thickness of 19.05 mm (0.75 in) and a total mass of 6.62 kg (weight of 14.6 lb). The panel with complex attachments and a typical piece of electronic equipment are shown in Figs. 5 and 6, respectively, and are representative of common flight hardware. The individual complex attachment mass (weight) values, starting in the upper left corner in Fig. 5 and moving clockwise, are 2034 g (4.48 lb)/1827 g (4.03 lb)/773.0 g (1.70 lb)/1195 g (2.63 lb)/1327 g (2.92 lb). The panel with simple attachments, with the same approximate spatial distribution as the complex attachment configuration, is shown in Fig. 7. For the configurations initially tested

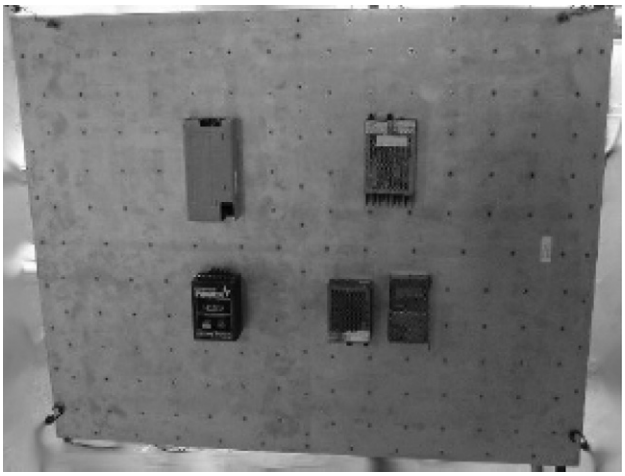

Fig. 5. 1.52 m by 1.22 m (5 ft by 4 ft) panel with 6.8 kg (15 lb) of complex attachments (electronic equipment). The panel is supported in the reverberation room at its four corners using low frequency elastic supports.

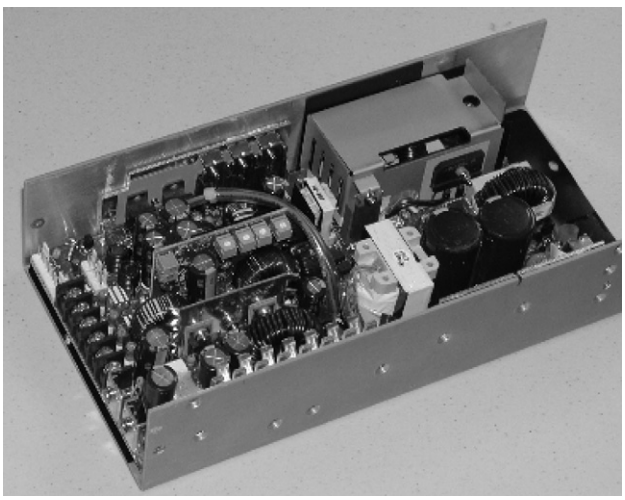

Fig. 6. Photograph showing the internals of a typical electronic box (complex attachment) with approximate mass of 2.0 kg (weight 4.48 lb).

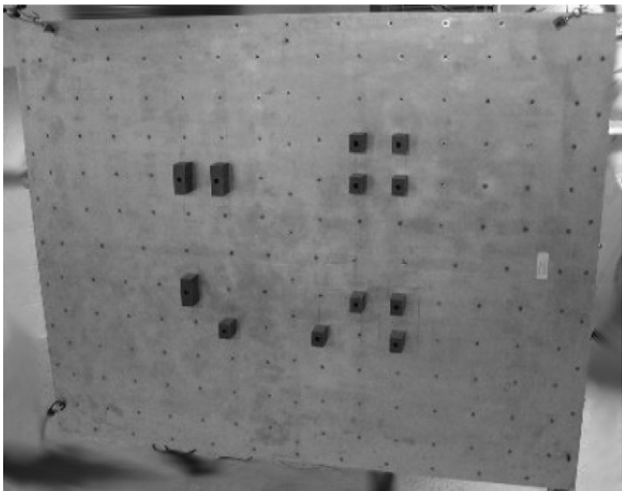

Fig. 7. Panel with 6.8 kg (15 lb) of simple attachments (lumped mass attachments).

in this investigation, the total attachment mass 6.8 kg (weight 15 lb) is approximately equal to the underlying panel structure mass. A detailed summary of the structural and mass properties is given in Table 1. In general, the 1.52 m (60.0 in) fixed panel width can be extended to 2.3 m (90 in) or even 2.8 m (110 in) on some communications satellite equipment panels (the fixed panel extent is ultimately limited by the launch vehicle payload fairing size). The 1.52 m dimension was chosen for this investigation to be representative of full scale flight hardware while still being of a size that can be readily handled in the laboratory as well as not requiring (costly) special tooling/manufacturing.

2.2. Steady-state model description

The statistical energy analysis power balance matrix equation [22] for two coupled subsystems can be written, using a modal power (energy/modal density) form, as

$$\begin{bmatrix} (\beta_{11}+\beta_{12}) & -\beta_{21} \\ -\beta_{12} & (\beta_{22}+\beta_{21}) \end{bmatrix} \begin{Bmatrix} \varphi_1 \\ \varphi_2 \end{Bmatrix} = \begin{Bmatrix} W_1 \\ W_2 \end{Bmatrix}, \tag{1}$$

where β_{ii} is the internal damping factor of the ith subsystem ($\beta_{ii} = \omega\eta_{ii}n_i$), β_{ij}, the coupling factor from the ith to the jth subsystem ($\beta_{ij} = \beta_{ji}$, $\beta_{ij} = \omega\eta_{ij}n_i$), η_{ii}, the internal damping loss factor of the ith subsystem, η_{ij}, the coupling loss factor from the ith to the jth subsystem, φ_i, the total space–time average modal power of subsystem i, $\varphi_i = E_i/n_i$, W_i, the time averaged external power input into subsystem i, E_i, the total space–time average response energy of subsystem i, n_i, the modal density of subsystem i and ω, the band center frequency (rad/s). Note that all quantities in Eq. (1) are frequency dependent ($\beta(\omega)$, $\eta(\omega)$, $\varphi(\omega)$, $E(\omega)$, $n(\omega)$, $W(\omega)$), however for brevity this will only be shown explicitly when additional clarification is needed.

There are several practical benefits in using the modal power form in this experimental investigation over that of the traditional energy form. First and foremost, the panel system response can be related directly to the modal power without the need to assume the complex system mass or effective mass. This comes about because in this form the measured conductance can be used and thus the modal density and mass need not be defined individually. Also, the coupling factors are reciprocal (the coupling matrix is symmetrical) and the internal (β) loss factors are equivalent to a form of the subsystem modal overlap factor.

For a room/acoustic volume (subsystem 1) and a panel/structure (subsystem 2) the modal powers become

$$\varphi_1 = E_1/n_1 = \frac{V_1\langle \bar{p}_1^2 \rangle}{\rho c^2 n_1}, \tag{2}$$

Table 1
Test structure and attachment properties.

Item	Value	Units (in–lb–s)	Value	Units (m–kg–s)
Panel facesheets				
Material (Al alloy 2024-T81)				
Thickness	0.012	in	3.048E−04	m
Modulus of elasticity (E)	1.05E+07	psi	7.239E+10	Pa
Density	0.101	lb/in^3	2.796E+03	kg/m^3
Poisson's ratio	0.33	–	0.33	–
Panel core				
Material (Al alloy 3/16-5056-0.0007)				
Thickness (approximate)	0.726	in	1.844E−02	m
G (L—ribbon, shear modulus)	27,000	psi	1.862E+07	Pa
G (W—warp, shear modulus)	13,000	psi	8.963E+07	Pa
Density	1.157E−03	lb/in^3	3.204E+01	kg/m^3
	2.0	lb/ft^3		
Total panel thickness	0.75	in	1.905E−02	m
Panel width/length dimensions				
Width (W—warp, perpendicular to core ribbon)	60.0	in	1.524E+00	m
Length (L—longitudinal, parallel to core ribbon)	48.0	in	1.219E+00	m
Calculated panel facesheets and core (weight/mass)	9.40	lb	4.264E+00	kg
Facesheets to core adhesive (approximately 0.040 lb/ft^2)	0.80	lb	3.629E−01	kg
202 inserts + adhesive (approximately 0.01605 lb/inserts)	3.24	lb	1.470E+00	kg
Edge treatment (approximately 0.064 lb/ft)	1.16	lb	5.262E−01	kg
Measured panel weight/mass (w/adhesive, inserts)	14.6	lb	6.622E+00	kg
Measured panel area weight/mass density	5.069E-03	lb/in^2	3.564E+00	kg/m^2
	0.73	lb/ft^2	–	–
Attachment added weight/mass				
Complex electronic attachments	15.8	lb	7.167E+00	kg
Lumped mass attachments	15.7	lb	7.121E+00	kg

where φ_1 is the room/acoustic volume modal power, E_1, the room/acoustic volume total space–time average response energy, n_1, the calculated acoustic volume (room) modal density, V_1, the measured room volume, $\langle \bar{p}_1^2 \rangle$, the measured acoustic volume space–time average mean square pressure, ρ, the acoustic medium (air) density (1.21 kg/m^3), c, the acoustic medium speed of sound (343 m/s) and

$$\varphi_2 = E_2/n_2 = \frac{\pi \langle \bar{v}_2^2 \rangle}{2\langle G_2 \rangle}, \tag{3}$$

where φ_2 is the panel modal power, E_2, the panel structure total space–time average response energy, n_2, the panel structure modal density, $\langle \bar{v}_2^2 \rangle$, the measured panel structure space–time average mean square velocity and $\langle G_2 \rangle$, the measured panel structure space averaged conductance.

The subsystem space averaged conductance is defined as

$$\langle G_2 \rangle = \frac{\pi}{2}\frac{n_2(\omega)}{M} = \frac{n_2(f)}{4M} = \text{measured Re\{vel/force\} mobility}, \tag{4}$$

where M is the structure mass.

For the experiment shown in Fig. 8 with power injected into the panel subsystem, Eq. (1) leads to the following important parameter definitions. The radiation coupling ($\beta_{21} = \beta_{\text{rad}}$), between the panel and room,

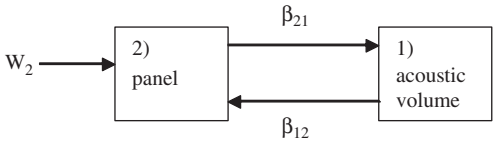

Fig. 8. Power injection experiment for a coupled panel and acoustic volume. The panel structure (no attachments), panel with simple attachments and the panel with complex attachments are all tested in the same fashion.

based on the measured modal powers and room internal damping factor, is

$$\beta_{21} = \beta_{\text{rad}} = \frac{\beta_{11}}{\left(\frac{\varphi_2}{\varphi_1} - 1\right)} = \frac{2}{\pi}\langle G_2\rangle R_{\text{rad}}, \tag{5}$$

where R_{rad} is the panel radiation resistance $= \rho c A_2 \sigma_{\text{rad}}$, A_2 , the panel radiating surface area, for un-baffled panel $= 2 \times$ surface area, σ_{rad}, the panel radiation efficiency, $\beta_{11} = \omega\eta_{11}n_1$, the measured in isolation room internal damping factor (from separate decay rate measurements), $\eta_{11} = 13.82/\omega T_{60}$, the room internal damping loss factor, T_{60}, the measured room reverberation time, $n_1 = V_1\omega^2/2\pi^2c^3$, the calculated room modal density and the remaining parameters are as previously defined.

When the panel modal power (the driven subsystem) is much greater than the room modal power, a condition which is generally true for the experiment depicted in Fig. 8, Eq. (5) reduces to

$$\beta_{21} \approx \frac{\varphi_1}{\varphi_2}\beta_{11}, \quad \left(\frac{\varphi_2}{\varphi_1} \gg 1\right) \tag{6}$$

and the radiation efficiency becomes

$$\sigma_{\text{rad}} \approx \frac{\omega V_1 \eta_{11}}{\rho^2 c^3 A_2}\frac{\langle \bar{p}_1^2\rangle}{\langle \bar{v}_2^2\rangle}, \tag{7}$$

which is independent of both the room modal density and the panel conductance (or modal density). This result means that, if the ratio of modal powers or modal energies is much greater than one, the radiation efficiency calculation will not be sensitive to potential errors in the room modal density or panel conductance. In addition, this is beneficial from an experimental point of view, since the measured dynamic quantities in Eq. (7) are the more straight forward to confidently obtain.

The panel structure internal damping factor based on the measured modal powers, measured panel structure power input W_2 and the computed/measured radiation coupling is

$$\beta_{22} = \beta_{21}\left(\frac{\varphi_1}{\varphi_2} - 1\right) + \frac{W_2}{\varphi_2}. \tag{8}$$

Eq. (8) applies to both the panel with no attachments as well as to the panel with simple (non-resonant lumped-mass) attachments. For the panel with complex attachments the damping factor can be expressed as

$$\beta_{22\text{-}s} = \beta_{22} + \beta_{s\text{-equip}}, \tag{9}$$

where $\beta_{s\text{-equip}}$ is the added losses due to the coupled resonant attachments (complex panel internals).

The panel induced damping (or loss) factor is simply the sum of the internal (β_{22} or $\beta_{22\text{-}s}$) and radiation factors,

$$\beta_t = \beta_{22} + \beta_{21} = \frac{W_2}{\varphi_2}. \tag{10}$$

The induced loss factor (β_t) is a meaningful ratio of dimensionless dynamic quantities and can take on values significantly greater than unity, however it is not a true loss factor [15]. It should also be noted that the damping factor ($\beta_{22\text{-}s}$) of the panel with complex attachments is actually an induced loss factor itself, however

for this investigation it is treated as an internal loss factor since the loaded panel system is characterized by averaged measurements made solely on the panel structure (not to any of the attachment internals). The true effective loss factor of the system relates the in situ external input power to the total system energy and would take the form

$$\beta_e \propto \frac{W_e}{\sum \varphi_i}, \tag{11}$$

where W_e is the external input power (in the experiment described here $W_e = W_2$). Unlike the induced damping factor, the effective damping factor is bounded with asymptotic limits of the "in isolation" factors of the coupled subsystems. The induced damping factor can take on potentially large values when much of the total system energy is stored in the attached subsystem (the vibration absorber effect). The induced and effective damping factors can also be affected by changes in the external input power due to the subsystem couplings [15]. This concept of effective or induced damping was described conceptually and analytically by Maidanik [8,9] and Brooks and Maidanik [10] and in the experimental power injection context by Bies and Hamid [11], Clarkson and Pope [23], Ranky and Clarkson [24] and Sun and Richards [12].

For the steady-state power injection evaluations in this investigation, the key quantities to be characterized and compared are the internal and induced damping losses. These quantities are calculated as given by Eqs. (8)–(10), using the raw measured response accelerations and pressures.

3. Measurements

This section presents the measurement techniques and their results. Implementation details for the structure conductance, critical to the modal power formulation and the structural acoustic power injection measurements are presented. The input force and output acceleration signals are sampled using a spectrum analyzer. The sample rate, block size and total time record are selected to be suitable to produce spectral estimates with acceptable random and bias errors [25]. To obtain conductances, the measured force–acceleration frequency response functions (FRFs) are converted to force–velocity FRFs for the drive point measurements. For the power injection measurements, the drive point force–acceleration cross-spectrum is used to compute the input power and spatially distributed response accelerations are measured and used to estimate the space averaged velocity response. The fixed bandwidth narrow band results are converted into proportional (typically one-third octave) standard bands.

3.1. Conductance

The relationship between a structure's modal density and conductance (real part of the velocity/force mobility or characteristic admittance), as given in Eq. (4), was shown by Cremer et al. [26] (the results date to previous work done circa 1950 or earlier). Clarkson and Pope [23], Clarkson [27,28] and Clarkson and Ranky [29] and their colleagues at the Institute of Sound and Vibration Research popularized the use of the modal density-average conductance relationship for experimentally characterizing modal densities of non-ideal systems where theoretical estimates are not readily available or not practical to develop. Norton [30] cited successful application of Eq. (4) to non-uniform structures with varying mass distributions using the total mass of the system. This concept was also applied to satellite non-homogeneous panel structures by Conlon et al. [31] and Conlon and Hambric [1]. Manning [32,33] has promoted the formulation of statistical energy analysis parameters using mobility functions along with using measured mobilities to improve statistical energy analysis models.

In this work Eq. (4) is applied to the panel structure with and without attachments. The measurements are made by applying broadband random noise excitation to the panel structures via a shaker/impedance head (B&K Model 8001 Impedance head with B&K charge amplifiers type 2635). Corrections are applied to the measured drive point mobility FRFs for transducer and attachment hardware mass/stiffness [34,35] (important for lightweight structures at high frequencies).

The three channel technique method popularized by Brown [36] and Brown and Norton [37] is used for measuring the drive point mobilities. This method has been shown to provide the best unbiased estimate of the

mobility, eliminating uncorrelated noise at both the input and output as well as minimizing resolution bias errors and the effects of shaker structure interaction. The experimentally estimated mobility is defined as

$$\hat{Y} = \frac{1}{j\omega}\hat{H}_i, \tag{12}$$

where $\hat{H}_i$ is the measured FRF, $\hat{H}_s = \hat{G}_{sa}/\hat{G}_{sf}$, the three channel technique FRF (cross-spectrum of shaker amp signal-acceleration $\hat{G}_{sa}$ divided by the cross-spectrum of shaker amp signal-force $\hat{G}_{sf}$, all uncorrelated "noise" is removed from both force and acceleration and resolution bias errors can be nearly eliminated thus allowing shorter time blocks of data to be used), $\hat{G}_{xy} = (1/m)\sum_{i=1}^{m}(P_{xy})_i$, the smoothed estimated cross-spectrum, (Bartlett's direct estimation procedure) and $P_{xy} = (2/T)[X_i^* Y]$, the raw individual single sided spectral computation (cross-spectral density) on time block i, the product of the Fourier transforms of the input $x(t)$ and output $y(t)$, the asterisk denotes the complex conjugate.

When measuring the mobility of lightweight structures and any structure at high frequencies, it is important to assess and compensate for any effects that the instrumentation has on the measurement itself. Refs. [37,38] give corrections for the effects of the added mass between the force transducer of the impedance head and the structure being measured. A typical impedance head and mounting is shown in Fig. 9 (note the accelerometer portion of the impedance head is not depicted but is located above the force transducer).

The "measured mass" corrected mobility is given as

$$Y_{\text{measured\_mass\_corrected}} = \frac{Y_{\text{measured}}}{1 - (j\omega M_a) Y_{\text{measured}}}, \tag{13}$$

where $Y_{\text{measured}} = (1/j\omega)H$ is the measured mobility (as a function of frequency), H, the measured force–acceleration FRF and M_a, the added mass between the force transducer and the structure, i.e. the driving platform and mounting screw.

The "spectral mass" corrected mobility is given as

$$Y_{\text{spectral\_mass\_corrected}} = \frac{Y_{\text{measured}}}{1 - \left(\dfrac{Y_{\text{measured}}}{Y_{\text{mass}}}\right)}, \tag{14}$$

where Y_{mass} is the measured mobility with the impedance head not attached to the structure but with any mounting hardware used from the impedance head to the structure, i.e. the impedance head driving the mounting screw. The spectral mass correction is shown to give improved results on lightweight structures at high frequencies and is applied to all the mobility data presented in this section.

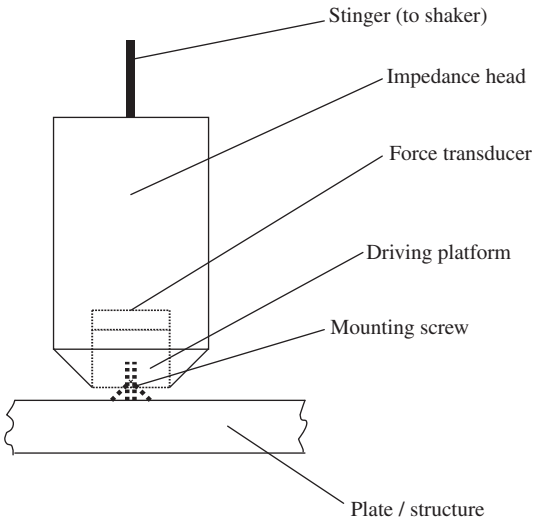

Fig. 9. Impedance head and attachment to structure. The impedance head is attached to the structure via a #10–32 screw.

Another aspect that can be of concern when measuring the point mobility in the fashion described is the drive contact area (i.e. the screw head diameter in Fig. 9) Theoretically, for a plate (considering transverse shear effects) driven with an ideal point force, the point response velocity becomes infinite due to shear deformation [26]. The force would "punch" a hole in the plate. Vér [39] gives simplified formulas and drive contact area applicability for point impedances. In a rigorous calculation considering a finite drive area this theoretical singularity can be eliminated. The theoretical plate results presented here use an approximation for the effective impedance (bending corrected for transverse shear effects at high frequencies via the effective wave speed and modal density [1]) which relies on the theoretical relationship between conductance, modal density and mass from Eq. (4). The impedance head is attached to the structure (for all applications discussed in this and subsequent sections) via a #10–32 screw as shown in Fig. 9, where the screw is screwed into the impedance head and glued to the structure with a thin layer of adhesive.

The drive point mobility measurement one-third octave band results are spatially averaged to obtain the band averaged point conductance measurements (13 drive points locations were used). Note the mobility measurements are acquired and processed into one-third octave band conductances up to 20 kHz, much higher in frequency than what will be used in the power injection experiments and models, in order to clearly identify any high frequency trends as compared to the theoretical infinite plate values. The power injection experiments and models will utilize the measured conductance results up to approximately 3 kHz. The conductance could be converted to modal density using the structure mass per Eq. (4). However, use of the conductance directly in the predictive model as shown in Eq. (3), avoids speculative generalizations on what mass to assume for the non-homogeneous structure.

Fig. 10 shows the space-averaged conductance measurement results for the panel structure (no attachments) and the panel with simple and complex attachments. The measurements are compared with the theoretical value [1] for the panel structure (no attachments). The panel structure results follow the theoretical trend well. The addition of the attachments to the panel has the most pronounced effect at the lower frequencies lowering the average conductance by approximately 1–3 dB in most bands below 1000 Hz as shown by the conductance ratio loaded/unloaded in Fig. 10c (the few bands where the loading increases the conductance are attributed to lower modal density of the unloaded panel and the shifting of modes into these bands when the panel is loaded). The panels with simple and complex attachments show similar results in conductance. At high frequencies (above approximately 1000 Hz) the average conductance for the panel structure and panel with attachments is approximately the same. This interesting result is expected theoretically because at these frequencies the panel has transitioned into shear dominated vibration where the conductance is independent of the attached mass (when the attached mass is treated as uniformly distributed limp mass the modal density increases linearly in proportion to the increased mass resulting in a constant ratio of modal density to mass thus a constant conductance per Eq. (4)).

These measured conductance results will be used in the vibroacoustic models for estimating the radiation efficiency, loss factors and induced loss factors.

3.2. Power injection: radiation efficiency, loss factor and induced loss factor

In these panel power injection experiments, the panel external input power (W_2) and response modal power (φ_2) and the reverberation room modal power (φ_1), are measured directly. The reverberation room has an approximate volume of 58 m^3 (2050 ft^3) and its loss factor (β_{11}) is measured in a separate reverberation time experiment. Recalling that the coupling factors are reciprocal ($\beta_{12} = \beta_{21}$), leaves two equations and two unknowns from Eq. (1), thus determining β_{21} and β_{22}, the radiation loss factor and internal (or effective internal $\beta_{22\text{-}s}$ for the panel with complex resonant attachments) loss factors.

As previously discussed, by recasting the power balance equation in this form, stressing the use of directly measured fundamental quantities, traditional sources of power injection errors can be reduced. Recall, one objective of this work is to treat the complex attachments as a spatially average entity whose effects on the underlying structural system must be observed and characterized from observations/measurements made on the underlying (panel) structure.

In experimental statistical energy analysis the response locations are generally chosen subjectively as a "random" spatial distribution. Rules of thumb for the number of structure responses are typically five per

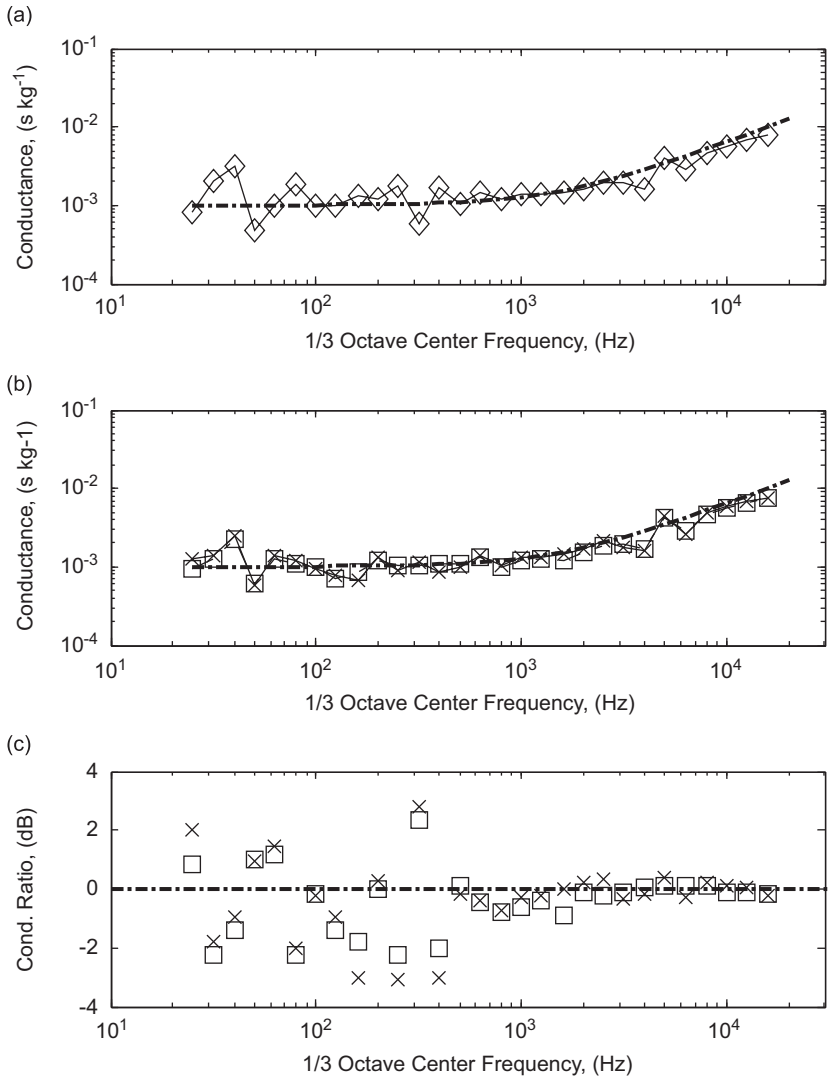

Fig. 10. Panel structure and panel with attachments measured space averaged conductance. The measurements are compared with the theoretical value for the panel structure: plot (a) (—◇— measured panel structure, —·— theory panel structure), plot (b) (---□--- measured panel with complex attachments, —×— measured panel with simple attachments, —·— theory panel structure). The panel structure compares well with the theoretical results, the addition of attachments has the most pronounced effect at the lower frequencies lowering the average conductance in most bands below 1000 Hz as shown by the conductance ratio loaded/unloaded and in plot (c) (□ measured panel with complex attachments, × measured panel with simple attachments).

(homogeneous) subsystem [40] using multiple random excitation points to simulate statistical independence of the driven modes [11]. For this investigation two panel structure drive excitation points (force and acceleration measured at the drive points) and a total of twelve different response locations (six for each drive) are used and the results averaged. The responses were measured using Dytran model 3035A accelerometers with a mass of 2.5 g each (3.25 g including mounting base) bonded to the structure. In addition, the reverberation room pressures are continuously spatially averaged with a traversing microphone (B&K Type 4133).

The panel power input is computed from the drive point impedance head measurements as

$$W_{2_{f1-f2}} = \int_{f1}^{f2} \mathrm{Re}\{\hat{G}_{fb}\}\,\mathrm{d}f, \tag{15}$$

where $\hat{G}_{fv} = (1/j\omega)\hat{G}_{fa}$ is the smoothed estimated force velocity cross-spectrum, $\hat{G}_{fa} = (1/m)\sum_{i=1}^{m}(P_{xy})_i$, the measured force acceleration cross-spectrum and $P_{xy} = (2/T)[X_i^* Y]$, the raw individual single sided spectral computation (cross-spectral density) on time block i.

The individual structure velocity responses are computed from the accelerometer measurements as

$$\hat{G}_{vv} = \frac{1}{(j\omega)^2}\hat{G}_{aa}, \tag{16}$$

where the smoothed estimated acceleration autospectral densities $\hat{G}_{aa}$ are calculated similarly as the cross-spectral densities using a single channel.

The two narrow band PI spectral measurements sets, input power/response pressure, are then converted into standard one-third octave values. Band averages or band totals can be used since the final parameter equations use ratios of the measured quantities. For the radiation coupling and efficiency the space–time averaged mean square pressure and velocity are used ($\langle\bar{p}_1^2\rangle/\langle\bar{v}_2^2\rangle$) (see Eqs. (5)–(7)). This one-third octave ratio is calculated for each of the two sets of data and then the ratios averaged to use in the power balance based parameter formulations. For the structure internal loss factor the same pressure/velocity ratio result is used in addition to the ratio ($W_2/\langle\bar{v}_2^2\rangle$) which is averaged from the two sets of data (see Eq. (8)).

An additional topic which can be of concern with response measurements on lightweight structures is the effects of the transducers, such as accelerometers, on the response of the structure. A rule of thumb that five times the impedance of the accelerometer (treated as a point mass) should not exceed the impedance of the structure to which it is mounted is generally acceptable. At higher frequencies, where this is generally of concern, the structure infinite plate impedance is often used. Comparisons of the theoretical and measured panel structure impedances (which correlate well to each other) and transducer (accelerometer) impedance magnitudes used in this investigation are shown to be approximately equal at 7000 Hz and the structure is five times the transducer up to 3000 Hz. Note the accelerometer/mounting hardware are treated as a lumped mass. This would indicate that transducer loading effects should not be significant below approximately 3000 Hz for the panel structure. With the heavier panel configurations with attachments this frequency range may extend even higher.

Fig. 11 shows the measured panel modal power is approximately 15 to over 1000 times higher than the room modal power, indicating that the approximations given in Eqs. (6) and (7) apply for both the panel structure (no attachments) and panel with simple and complex attachments power injection measurements. The panel radiation efficiency results are compared in Fig. 12. The estimated panel structure critical frequency, based on an infinite plate calculation, is approximately 560 Hz. If the attachments for the panel were treated as uniformly distributed limp mass, the corresponding infinite plate critical frequency would be approximately 900 Hz. The radiation efficiency falls off below the critical frequency with the general expected trend for an unbaffled plate. The radiation efficiencies also follow the expected trend near and above the critical frequency, with magnitudes that peak out slightly above 1.0 and then asymptotically return to 1.0 at higher frequencies. Of particular note is that the radiation efficiencies for all three panel configurations are nearly the same over most of the frequencies, with some variations at the lower frequencies. Fig. 13 shows similar trends for the panel radiation loss factors, as were shown for the radiation efficiencies. Recall from Eq. (5) the radiation loss factor is a function of the radiation efficiency and the average conductance.

The panel structure and panel with attachments measured internal damping factor and damping loss factor (which includes effects from the complex attachments) results are shown in Fig. 14. The measurements show that the panel with complex attachments has a significantly higher damping factor (β_{22}) over many of the frequency bands examined, which was anticipated since the effects of the resonant complex internals are included as was given in Eq. (9) for $\beta_{22\text{-}s}$. The damping loss factors (η_{22}), calculated using the total mass (panel structure + attachments), for the panel structure and panel with simple attachments follow a similar trend with magnitudes that could be expected from these types of practical structures, with a value of approximately 0.025 at the lower frequencies and rolling off proportional to $1/f$ at the higher frequencies. For the panel with complex attachments, the damping loss factor (η_{22}) shown is an induced loss factor and is significantly higher than the values for the other panels for the frequencies above 100 Hz. However, the (η_{22}) values for the panel with complex attachments shown would only be valid if the resonant attachment internals had the same space averaged mean square velocity response as that of the measured panel structure. The panel structure and panel

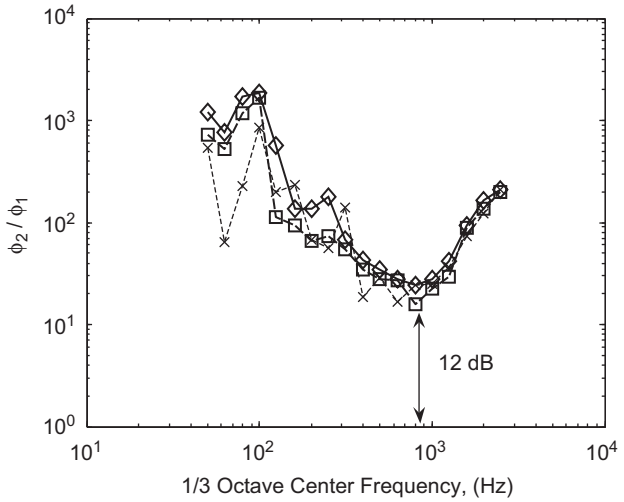

Fig. 11. Panel structure and panel with attachments ratios of modal power φ_2/φ_1 (panel/acoustic, - - - × - - - measured panel structure, - - - □ - - - measured panel with complex attachments, — ◇ — measured panel with simple attachments). When the panel modal power (the driven subsystem) is much greater than the room modal power, the expressions for the panel radiation loss factor and radiation efficiency are independent of both the room modal density and the panel conductance (or modal density), thus their results will not be sensitive to potential errors in the calculated room modal density or measured panel conductance.

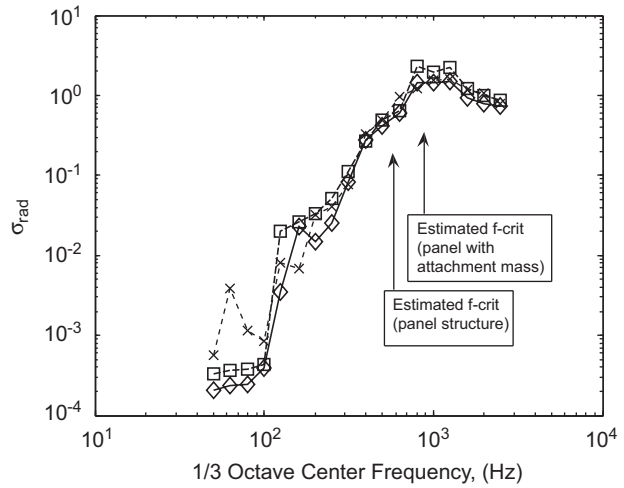

Fig. 12. Panel structure and panel with attachments measured radiation efficiency results (- - - × - - - measured panel structure, - - - □ - - - measured panel with complex attachments, — ◇ — measured panel with simple attachments). The measurements show the same trend above 100 Hz with the expected characteristics of an unbaffled plate (note the panel structure infinite plate critical frequency is calculated to be approximately 560 Hz and for the attachments treated as uniform limp mass loading the infinite plate critical frequency is approximately 900 Hz).

with attachments damping loss factors (η_{22}) can also be contrasted with measured electronic equipment modal damping loss factors of approximately $\eta_{ii} \approx 0.035 \pm 0.01$ over the frequency range of 100–400 Hz. These electronic equipment damping loss factors were measured with the equipment in isolation (from the panel) using input–output transfer functions from the external aluminum chassis to the internal circuit boards.

Fig. 15 shows the panel structure and panel with attachments measured induced loss factor results, representing panel damping induced by the structural acoustic coupling and by the resonant attachments (for the panel with complex attachments). The measurements show the induced loss factors to be roughly the same

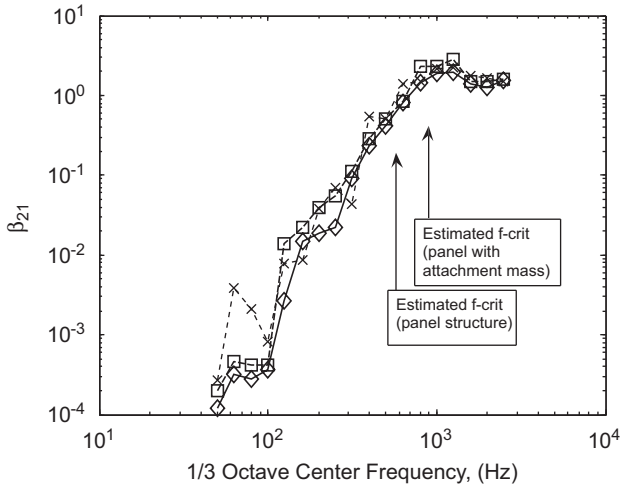

Fig. 13. Panel structure and panel with attachments measured radiation loss factor results (- - - × - - - measured panel structure, - - - □ - - - measured panel with complex attachments, — ◇ — measured panel with simple attachments). The measurements show a similar trend as the radiation efficiency results, with the radiation coupling of the unloaded and loaded panels being very similar over many of the frequency bands.

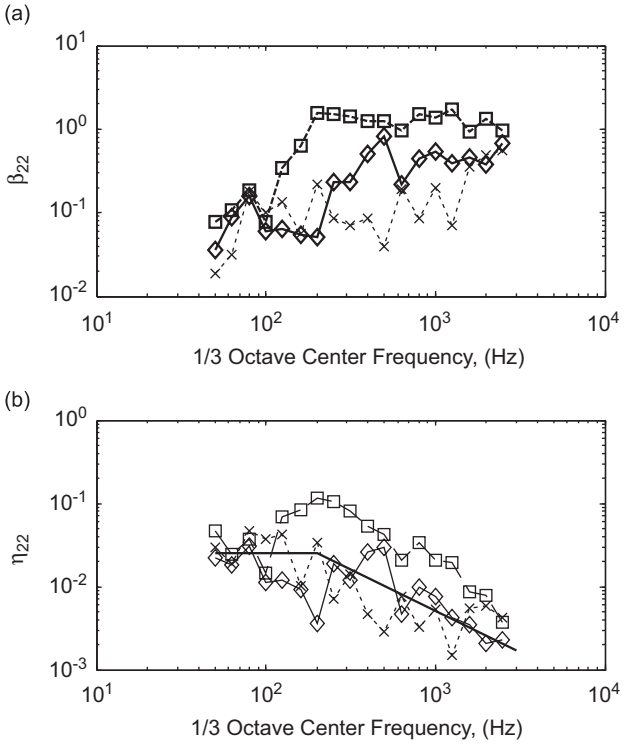

Fig. 14. Panel structure and panel with attachments measured internal damping factor: (a) and damping loss factor results and (b) (- - - × - - - measured panel structure, - - - □ - - - measured panel with complex attachments, — ◇ — measured panel with simple attachments). The measurements show that the complex equipment loaded panel has a significantly higher damping factor (β_{22}) over many of the frequency bands examined. The damping loss factors (η_{22}) are calculated using the total mass for the panel structure and panels with attachments.

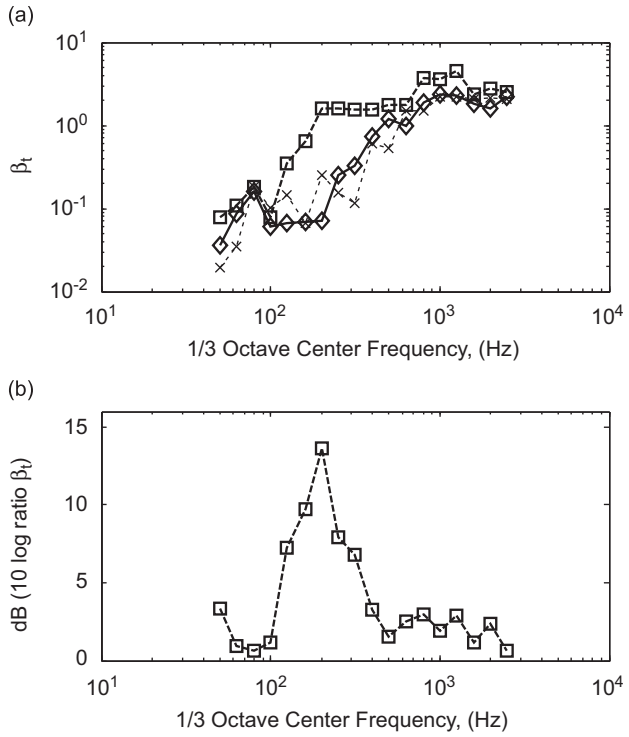

Fig. 15. Panel structure and panel with attachments measured induced loss factor results (β_t): plot (a) (- - - × - - - measured panel structure, - - -□- - - measured panel with complex attachments, —◇— measured panel with simple attachments) and plot (b) (- - -□- - - ratio of electronics loaded/mass loaded). The measurements show the induced loss factors to be roughly the same at the lower and higher frequencies. In the mid-frequencies the resonant internals of the complex attachments give rise to significantly higher induced damping levels over the frequencies from 100 to 500 Hz, with a maximum difference of approximately 14 dB at 200 Hz.

at the lower and higher frequencies (below 100 Hz and above 500 Hz). In the mid-frequencies, the resonant internals of the complex attachments give rise to significantly higher induced damping levels, with a maximum difference of approximately 14 dB at 200 Hz. These power injection induced damping results also correlate well to the trends shown by the decay curves in Figs. 3 and 4 for the panels with simple and complex attachments.

3.3. Design parameter results and procedures

Designers are frequently required to make preliminary assessments of hardware with similar traits to the structures evaluated in the earlier sections of this work. With this in mind, several additional complex attachment configurations are evaluated following the systematic procedures previously outlined. The goal is to gain additional insight useful for identifying underlying trends from a wider range of panel attachments encompassing variations of interest to designers and provide general parameter results and procedures that might be used for understanding and assessing other different configurations of interest. The important parameters to generalize are the structure average conductance, the radiation coupling or loss factor and the internal damping factor. The relative contributions to the total induced loss factor (radiation vs. internal) will also be important for understanding the response mechanisms of the systems, how important transition frequencies change for varying configurations and finally for developing approximations for the assessment of new designs.

Two additional configurations of the panel with complex attachments are evaluated with 21.3 kg (47 lb) and 32.2 kg (71 lb) of total attachments (the complex attachments were of similar construction as those previously described and spatially distributed on the panel). This results in measurement sets for four configurations; the

panel structure (no attachments) and the panel with approximately $1x/3x/5x$ the total complex attachment mass where "x" is equal to the approximate mass of the underlying panel structure.

Figs. 16 and 17 show the radiation efficiency and radiation loss factor results. The radiation efficiency is shown in max/min envelope form to emphasize the degree of variation between the four configurations (approximately 4–10 dB for most of the frequency bands between 100 and 1000 Hz). However, the results for radiation loss factor shown in Fig. 17 collapse well to a general trend for all four configurations. This general trend result could be used directly to estimate some new design's radiation loss factor, or the trend result could be used with the relationships given in Eqs. (4) and (5) to estimate the new design's radiation efficiency given its specific conductance (or modal density and mass).

Figs. 18–21 show the (total) induced loss factors (β_t) and the relative contributions from the internal damping (β_{22}, or $\beta_{22\text{-}s}$) and radiation coupling ($\beta_{21} = \beta_{\text{rad}}$) for the four configurations. Fig. 18 shows the results for the panel structure (no complex attachments), with the total losses being dominated by internal

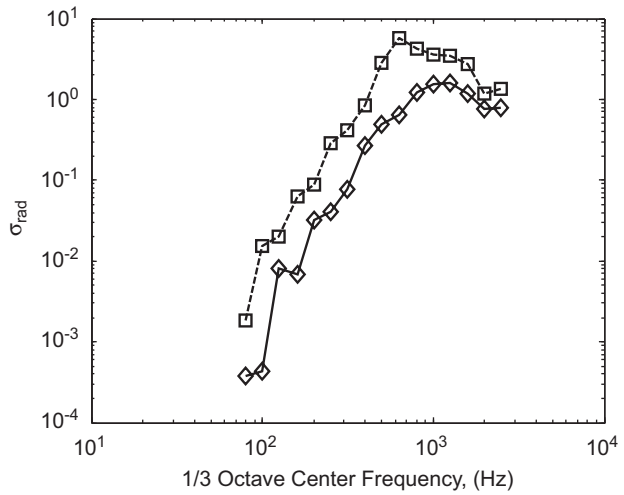

Fig. 16. Panel structure and panel with complex attachments measured radiation efficiencies (σ_{rad}), (- - -□- - - maximum envelope, —◇— minimum envelope). The spread between the max and min band values is approximately 4–10 dB for most of the frequency bands between 100 and 1000 Hz.

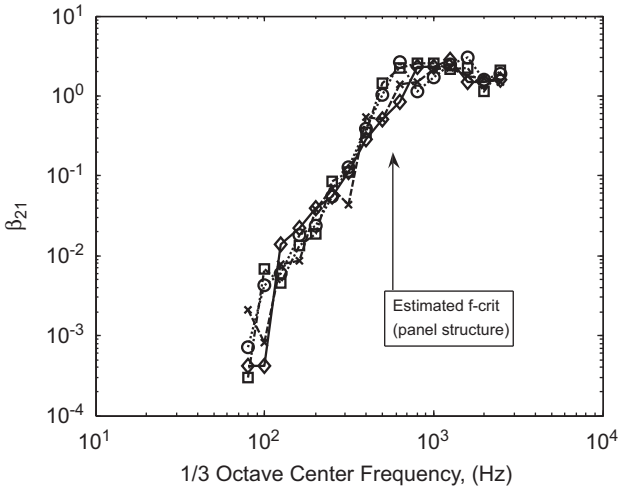

Fig. 17. Panel structure and panel with complex attachments measured radiation loss factors (β_{21}), (- - - × - - - panel structure, —◇— panel with $1x$ complex attachments, - -□- - panel with $3x$ complex attachments, - -o- - panel with $5x$ complex attachments). The results collapse well to a general trend for all four configurations.

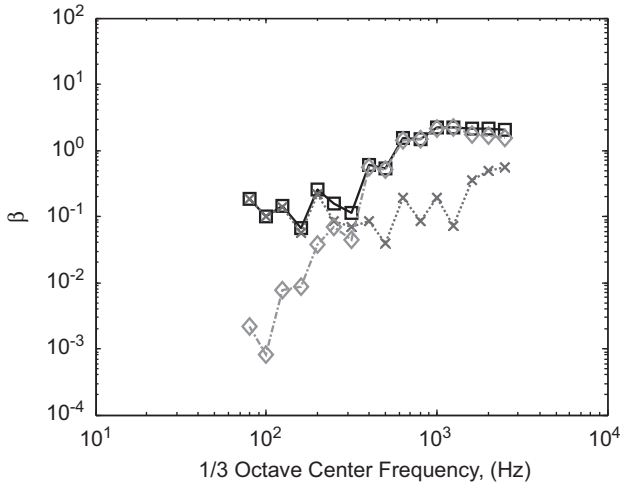

Fig. 18. Panel structure loss factors, (—□— induced loss factor (β_t), - - - × - - - internal damping factor (β_{22}), - - - ◇ - - - radiation loss factor). The results for the panel structure (no complex attachments) show the total losses being dominated by internal damping at low frequencies and then by radiation losses at higher frequencies. The transition between the two regions occurs at approximately one half the calculated critical frequency.

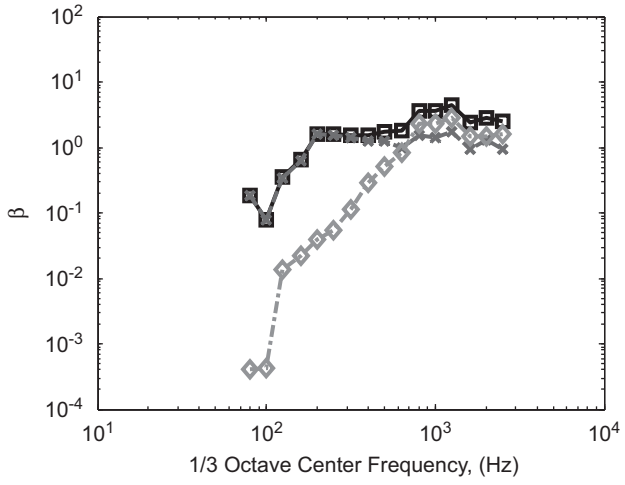

Fig. 19. Panel with ($1x$) complex attachments loss factors, (—□— induced loss factor (β_t), - - - × - - - internal damping factor ($\beta_{22\text{-}s}$), - - - ◇ - - - radiation loss factor). The results for the panel with complex attachments (attachment mass = panel structure mass), show that the induced damping transitions from internal to radiation losses at approximately the panel critical frequency. At the higher frequencies the internal damping (effects from the complex attachments) is not completely dominated by the radiation losses as was the condition for the panel structure only.

damping at low frequencies and then by radiation losses at higher frequencies. The transition between the two regions occurs at approximately one half the calculated critical frequency. Figs. 19–21 show the incremental effects of the complex attachments on the total and contributing losses ($1x/3x/5x$ total complex attachment mass). Fig. 19 shows, for the $1x$ complex attachment mass, that the induced damping transitions from internal to radiation losses at approximately the panel critical frequency. In this case however, at the higher frequencies the internal damping (effects from the complex attachments) is not completely dominated by the radiation losses as was the case for the panel structure shown in Fig. 18. Figs. 20 and 21 show that the $3x$ and $5x$ complex attachment mass configurations have induced losses that are completely dominated by the internal

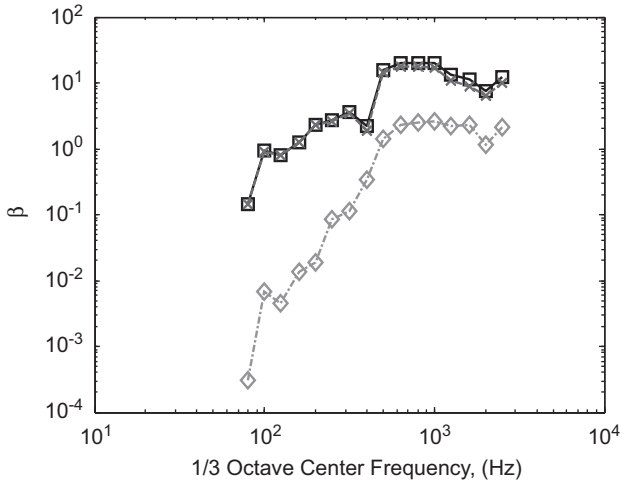

Fig. 20. Panel with (3x) complex attachments loss factors, (—□— induced loss factor (β_t), - - - × - - - internal damping factor ($\beta_{22\text{-}s}$), - - -◇- - - radiation loss factor). The results for the panel with complex attachments (attachment mass = three times the panel structure mass), shows induced losses that are completely dominated above 100 Hz by the internal damping due to the attachments (6–20 dB).

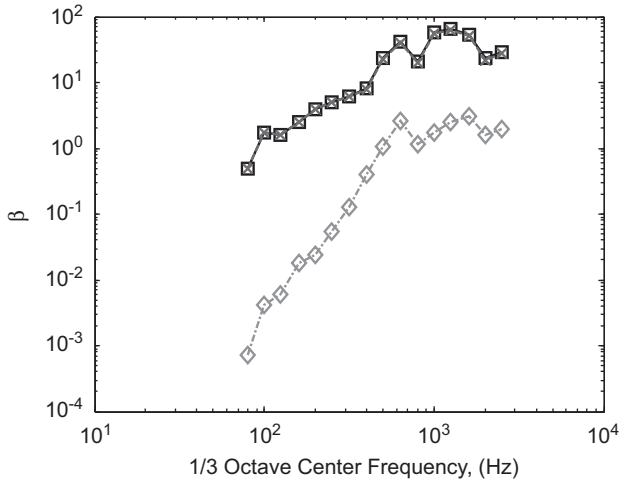

Fig. 21. Panel with (5x) complex attachments loss factors, (—□— induced loss factor (β_t), - - - × - - - internal damping factor ($\beta_{22\text{-}s}$) , - - -◇- - - radiation loss factor). The results for the panel with complex attachments (attachment mass = five times the panel structure mass), shows induced losses that are completely dominated above 100 Hz by the internal damping due to the attachments (12–25 dB).

damping due to the attachments (for the 3x configuration 6–20 dB and for the 5x configuration 12–25 dB at frequencies above approximately 100 Hz).

These results indicate a transition when the complex attachment mass is approximately equal to that of the underlying structure. In this region both internal damping and radiation losses can control the system overall losses (and thus vibration response). Above this region, with higher total complex attachment mass, the system total induced losses can be approximated by the internal damping and the radiation losses may be ignored. The measured space averaged conductance trends were similar to those shown previously in Fig. 10b with a bending region and a transition to shear at the higher frequencies. The infinite plate calculated values, treating the attachment mass as uniformly distributed limp mass, could be used as a conductance lower limit in the bending region and as the approximate conductance in the shear dominated region.

The internal damping factors, (β_{22}) or ($\beta_{22\text{-}s}$), for all four configurations are plotted in Fig. 22 showing how the damping factor varies with respect to both total attachment mass and frequency. The trends

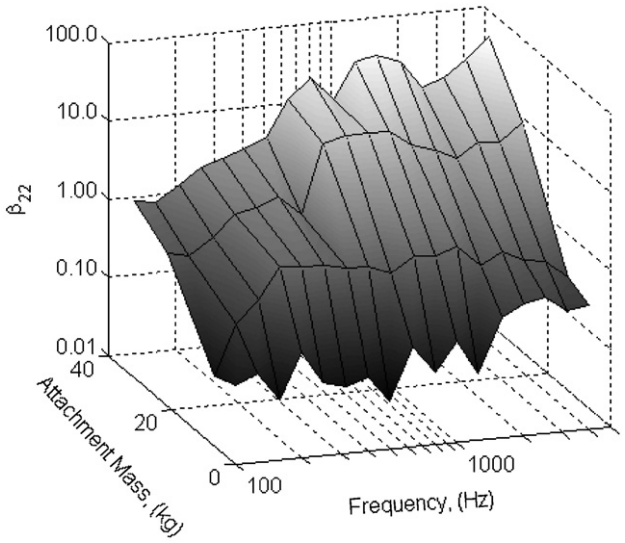

Fig. 22. Measured internal damping factors (panel structure and panel with complex attachments). Conditions for varying frequencies and complex attachment total mass are shown.

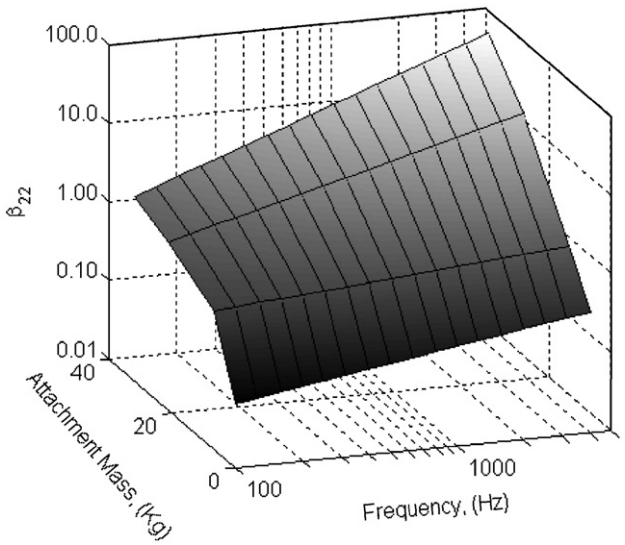

Fig. 23. Internal damping factor curve fit (panel structure and panel with complex attachments). A linear fit on log-frequency and log-(β) is assumed; conditions for varying frequencies and complex attachment total mass are shown.

approximately follow a linear on log-frequency and log-damping relationship. Fig. 23 shows the simple fit results for the measurements in Fig. 22 (assuming a linear on log-frequency and log-damping relationship). These simplified trend results put the internal damping factor in a form more readily usable by designers.

For the assessment of new designs with similar configurational traits the following process can be used. Where unique conductance results are not available, use the infinite plate calculated values with the attachment mass treated as uniformly limp mass. Estimate the radiation loss factor from Fig. 17. If the new panel cross-section critical frequency is significantly different than the panel structure used in this investigation, the Fig. 17 results can be frequency shifted for the new design. Lastly, estimates for the internal damping can be taken from Fig. 24, based upon the ratio of complex attachment mass to panel structure mass.

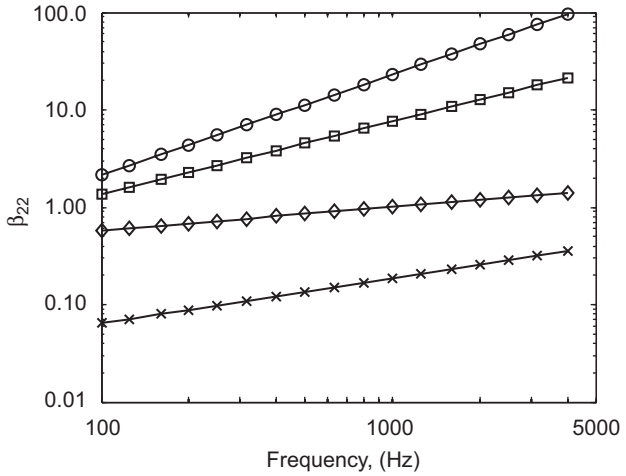

Fig. 24. Internal damping factor design curve, (— × — panel structure, —◇— attachment mass = structure mass, —□— attachment mass = 3*x* structure mass, —o— attachment mass = 5*x* structure mass). Conditions for varying frequencies and ratios of complex attachment mass to structure mass are shown.

4. Conclusions

This work has experimentally investigated the critical vibroacoustic response characteristics of a class of lightweight structures representative of those used in communications satellites. A model framework for critical vibroacoustic parameter interpretations was established, experimental procedures developed and parametric trends have identified and contrasted for structures with simple (non-resonant lumped mass) attachments and for complex (resonant electronic equipment) attachments. For the initial assessments, with the attachment mass approximately equal to the structure mass, the panel attachment effects were minimal in terms of changes in the radiation efficiency/coupling and space averaged conductance. However, the induced damping for the panel with complex attachments was up to 14 dB higher than that for the panel with simple attachments. Unlike related previous works where the attachments' mass was typically on the order of ten percent of the primary structure mass, in this investigation the minimum total loaded structure mass is approximately twice that of the underlying sandwich panel mass.

The critical parameters investigated include the average system conductance (related to modal density and thus energy storage), radiation efficiency (related to the structural acoustic coupling and thus input energy from an external acoustic field as well as output acoustically radiated energy) and damping (proportional to the energy dissipated). The results and methods of this work can be used to develop improved predictive models for this class of complex structures. The critical modeling parameters have been identified and quantified: average conductance, radiation coupling and induced damping. Comparisons to well established theoretical results for finite and infinite systems were made for reference, in particular showing the important role of transverse shear in the panel conductance above approximately 1000 Hz.

The internal loss factor results show the role internal and radiation losses play in the total induced loss factor including the effects of both resonant and non-resonant attachments. For the panel structure alone and the panel with simple attachments, the radiation losses play a significant role over much of the frequency spectrum, especially near and above the critical frequency. With just a few complex attachments this situation changes significantly, showing that over much of the mid-frequency spectrum (100–500 Hz) the effects of the resonant complex attachments are the limiting loss mechanism. With the critical parameter characterizations from this study, applied to predicting the vibration responses of these complex structures, vibroacoustic engineers can now take the next step and use their new models to identify where vibration control development is required.

General design parameter results and recommended design assessment procedures are given based on the evaluation of several complex attachment configurations to gain additional insight useful for identifying

underlying trends encompassing variations of interest to designers. The resulting measurement sets include four configurations; the panel structure (no attachments) and the panel with approximately $1x/3x/5x$ the total complex attachment mass where "x" is equal to the approximate mass of the underlying panel structure.

Future work will be focused in two important areas to expand on the results presented in this work. The first is to continue the steady-state power injection based parametric investigation to include a wider range of panel attachment masses and underlying structure properties to encompass variations of interest to designers. The second area to be investigated will explore quasi-transient models and their use with decay measurements such as shown in Figs. 3 and 4, to see if the critical response parameters developed with the power injection experiments could also be developed using a transient model and potentially more simplified decay measurements. The use of quasi-transient statistical energy analysis formulations for parameter determinations was proposed by Maidanik [8,9] and solutions for two coupled systems developed by Sun et al. [13]. More recently Pan and Bies [41] and Sum [42] have applied the quasi-transient statistical energy analysis approach to several practical problems in noise and vibration. It is along these lines that the quasi-transient statistical energy analysis approach will be explored for application to the study of simple and complex loaded panels.

References

[1] S.C. Conlon, S.A. Hambric, Predicting the vibroacoustic response of satellite equipment panels, *Journal of the Acoustical Society of America* 113 (3) (2003) 1455–1474.
[2] Structural Acoustics Design Manual, European Space Agency, ESA PSS-03-204, March 1996.
[3] C. Soize, Probabilistic structural modeling in linear dynamic analysis of complex mechanical systems: I Theoretical elements, *Recherche Aerospatiale (English Edition)* 5 (1986) 23–48.
[4] A.D. Pierce, V.W. Sparrow, D.A. Russell, Fundamental structural-acoustic idealizations for structures with fuzzy internals, *Journal of Vibration and Acoustics* 117 (1995) 339–348.
[5] M. Strasberg, D. Feit, Vibration damping of large structures induced by attached small resonant structures, *Journal of the Acoustical Society of America* 99 (1996) 335–344.
[6] Y.K. Lin, On the standard deviation of change-in-impedance due to fuzzy subsystems, *Journal of the Acoustical Society of America* 101 (1) (1997) 616–618.
[7] R.S. Langley, P. Bremner, A hybrid method for the vibration analysis of complex structural–acoustic systems, *Journal of the Acoustical Society of America* 105 (3) (1999) 1657–1671.
[8] G. Maidanik, Response of coupled dynamic systems, *Journal of Sound and Vibration* 46 (4) (1976) 561–583.
[9] G. Maidanik, Some elements in statistical energy analysis, *Journal of Sound and Vibration* 52 (2) (1977) 171–191.
[10] J.E. Brooks, G. Maidanik, Loss and coupling loss factors of two coupled dynamic systems, *Journal of Sound and Vibration* 55 (3) (1977) 315–325.
[11] D.A. Bies, S. Hamid, In situ determination of loss and coupling loss factors by the power injection method, *Journal of Sound and Vibration* 70 (2) (1980) 187–204.
[12] J.C. Sun, E.J. Richards, Prediction of total loss factors of structures, I: theory and experiments, *Journal of Sound and Vibration* 103 (1) (1985) 109–117.
[13] H.B. Sun, J.C. Sun, E.J. Richards, Prediction of total loss factors of structures, III: effective loss factors in quasi-transient conditions, *Journal of Sound and Vibration* 106 (3) (1986) 465–479.
[14] G. Maidanik, J. Dickey, Design criteria for the damping effectiveness of structural fuzzies, *Journal of the Acoustical Society of America* 100 (1996) 2029–2033.
[15] G. Maidanik, J. Dickey, On the external input power into coupled structures, *Proceedings of the Symposium of Statistical Energy Analysis*, IUTAM, Southampton, England, 1997.
[16] G. Maidanik, K.J. Becker, Various loss factors of a master harmonic oscillator coupled to a number of satellite harmonic oscillators, *Journal of the Acoustical Society of America* 103 (1998) 3184–3195.
[17] G. Maidanik, K.J. Becker, Dependence of the induced loss factor on the coupling forms and coupling strengths: linear analysis, *Journal of Sound and Vibration* 266 (2003) 15–32.
[18] G. Maidanik, K.J. Becker, Dependence of the induced loss factor on the coupling forms and coupling strengths: energy analysis, *Journal of Sound and Vibration* 266 (2003) 33–48.
[19] G. Maidanik, Induced damping by a nearly continuous distribution of nearly undamped oscillators: linear analysis, *Journal of Sound and Vibration* 240 (4) (2001) 717–731.
[20] A. Akay, Z. Xu, Experiments on vibration absorption using energy sinks, *Journal of the Acoustical Society of America* 118 (5) (2005) 3043–3049.
[21] I. Murat Koc, A. Carcaterra, Z. Xu, A. Akay, Energy sinks: vibration absorption by an optimal set of undamped oscillators, *Journal of the Acoustical Society of America* 118 (5) (2005) 3031–3042.
[22] R.H. Lyon, R.G. DeJong, *Theory and Application of Statistical Energy Analysis*, second ed., Butterworth-Heinemann, Boston, 1995.

[23] B.L. Clarkson, R.J. Pope, Experimental determination of modal densities and loss factors of flat plates and cylinders, *Journal of Sound and Vibration* 77 (4) (1981) 535–549.
[24] M.F. Ranky, B.L. Clarkson, Frequency average loss factors of plates and shells, *Journal of Sound and Vibration* 89 (3) (1983) 309–323.
[25] J.S. Bendat, A.G. Piersol, *Random Data Analysis and Measurement Procedures*, third ed., Wiley Inter-science, Wiley, New York, 2000.
[26] L. Cremer, M. Heckl, E.E. Ungar, *Structure-Borne Sound, Structural Vibrations and Sound Radiation at Audio Frequencies*, Springer, Berlin, Heidelberg, New York, 1973.
[27] B.L. Clarkson, The derivation of modal densities from point impedances, *Journal of Sound and Vibration* 77 (4) (1981) 583–584.
[28] B.L. Clarkson, Experimental determination of modal density, in: I. Elishakoff, R.H. Lyon (Eds.), *Random Vibration—Status and Recent Developments*, Elsevier, Amsterdam, Oxford, New York, Tokyo, 1986 (Chapter 5).
[29] B.L. Clarkson, M.F. Ranky, Modal density of honeycomb plates, *Journal of Sound and Vibration* 91 (1) (1983) 103–118.
[30] M.P. Norton, *Fundamentals of Noise and Vibration Analysis for Engineers*, Cambridge University Press, Cambridge, 1989.
[31] S.C. Conlon, S.A. Hambric, J.E. Manning, Computational evaluation of satellite equipment panel modal densities and radiation efficiencies, *Proceedings of NOISE-CON 2000*, *Joint ASA/NOISE-CON Meeting*, Newport Beach, CA, 2000.
[32] J.E. Manning, Formulation of SEA parameters using mobility functions, *Philosophical Transactions of the Royal Society London* 346 (1994) 477–488.
[33] J.E. Manning, Use of measured mobility to improve SEA predictions in the mid-frequency range, *Proceedings of DETC99, 17th ASME Biennial Conference on Mechanical Vibration and Noise*, Las Vegas, NV, 1999.
[34] K.T. Brown, M.P. Norton, Some comments on the experimental determination of modal densities and loss factors for statistical energy analysis applications, *Journal of Sound and Vibration* 102 (4) (1985) 588–594.
[35] P.R. Keswick, M.P. Norton, A comparison of modal density measurement techniques, *Applied Acoustics* 20 (1987) 137–153.
[36] K.T. Brown, Measurement of modal density: an improved technique for use on lightly damped structures, *Journal of Sound and Vibration* 96 (1) (1984) 127–132.
[37] K.T. Brown, M.P. Norton, Some comments on the experimental determination of modal densities and loss factors for statistical energy analysis applications, *Journal of Sound and Vibration* 102 (4) (1985) 588–594.
[38] P.R. Keswick, M.P. Norton, A comparison of modal density measurement techniques, *Applied Acoustics* 20 (1987) 137–153.
[39] I.S. Vér, Interaction of sound waves with solid structures, in: L.L. Beranek, I.S. Vér (Eds.), *Noise and Vibration Control Engineering, Principles and Applications*, Wiley Inter-Science, Wiley, New York, 1992 (Chapter 9).
[40] N. Lalor, The experimental determination of vibrational energy balance in complex structures, *Proceedings SIRA Conference on Stress and Vibration*, Paper No. 108429, London, 1989.
[41] J. Pan, D.A. Bies, The effect of fluid-structural coupling on acoustical decays in a reverberation room in the high-frequency range, *Journal of the Acoustical Society of America* 87 (2) (1990) 718–727.
[42] K.S. Sum, Use of statistical energy analysis for the prediction of Sabine absorption coefficient of modally reactive panels, *Journal of the Acoustical Society of America* 116 (3) (2004) 1596–1606.